Table I. Characteristics of Diarylcarbenium Ions

substituents			via diarylcarbenes			via photoheterolysis		
4-	4'-	solvent	precursor	λ_{max}, nm	k,[a] s^{-1}	precursor	λ_{max},[f] nm	k,[g] s^{-1}
MeO	MeO	AN-W[e] (1:2)	Ar_2CN_2	500	$(1.2 \pm 0.1) \times 10^5$	Ar_2CHOAc	500	1.3×10^5
MeO	H	AN-W (1:4)	Ar_2CN_2	455	$(2.3 \pm 0.1) \times 10^6$	Ar_2CHOAc	455	2.1×10^6
Me	Me	AN-W (1:2)	Ar_2CN_2	462	$(4.2 \pm 0.1) \times 10^7$	Ar_2CHOAr[c]	460	3.2×10^7
H	H	TFE[d]	tetraphenyl oxirane	435	$(3.2 \pm 0.1) \times 10^6$	Ar_2CHOAr[c]	440	3.2×10^6
		AN-TFE (1:1.6)	Ar_2CN_2	430	$(6.6 \pm 0.2) \times 10^6$	Ar_2CHCl	435[e]	6.8×10^6
Cl	Cl	AN-TFE (1:1.6)	Ar_2CN_2	470	$(5.9 \pm 0.1) \times 10^6$	Ar_2CHCl	472[e]	7.0×10^6

[a] At 20 ± 2 °C. [b] Acetonitrile–water. [c] OAr = 4-cyanophenyl ether. [d] 2,2-Trifluoroethanol. [e] In acetonitrile. [f] References 11 and 17. [g] Reference 11 and 13.

work to identify the transients derived from diarylcarbene precursors. LFP (248 nm, 20-ns pulses) of 4,4'-dimethoxydiphenyldiazomethane in acetonitrile–water gave rise to virtually the same transient absorption as that obtained by photoheterolysis of Ar_2CHX[11,13,17] (Figure 1 and Table I). The decay of the transient was first-order, the rate constant being unaffected by oxygen and independent of the precursor concentration. Corroboration was provided by the use of time-resolved conductivity detection in weakly basic solution. The observed steep increase in conductance after the pulse (Figure 1) is due to protonation of the carbene by H_2O to give the carbenium ion and OH^-. The subsequent decrease in conductance is caused by reaction of the cation with the solvent, neutralizing OH^-. LFP of 4-methoxy- and 4,4'-dimethyldiphenyldiazomethane in acetonitrile–water also generated diarylcarbenium ions whose absorption and reactivity were in good agreement with previous measurements[11,13] (Table I).

The reaction rate of the parent diphenylcarbenium ion is too fast to be measured in acetonitrile–water but is conveniently monitored in the less nucleophilic solvent 2,2,2-trifluoroethanol (TFE). The acidity of TFE (pK_a = 12.4), however, induces decomposition of diphenyldiazomethane. Therefore, solutions of diphenyldiazomethane in acetonitrile were mixed with TFE in a flow system ca. 10 s prior to LFP. Tetraphenyloxirane, unaffected by TFE, was used as an alternative source of diphenylcarbene.[18] The transient spectra and rates thus obtained identify the diphenylcarbenium ion unambiguously. 4,4'-Dichlorodiphenylcarbenium ion was generated similarly from the analogous diazo compound (Table I).

Diarylcarbenium ions covering a reactivity range (with water) of 10^7 have thus been shown to arise from carbenic precursors by protonation with OH groups. In contrast, LFP of 9-diazofluorene in 1,1,1,3,3,3-hexafluoro-2-propanol (HFIP) did not provide the transient spectrum of 9-fluorenyl cation[14] (which is readily observed following LFP of 9-fluorenol in HFIP).[19] In analogy with cyclopentadienylidene,[7] and in accordance with the low basicity of its "aromatic" singlet state, 9-fluorenylidene is not protonated by a solvent as acidic as HFIP (pK_a = 9.3).

In all successful experiments, the absorption spectra of diarylcarbenium ions evolved within the 20-ns laser pulse. Rapid formation of the carbocations is consistent with the rates (10^9–10^{10} M^{-1} s^{-1}) at which singlet diphenylcarbene is quenched by ROH.[10,20] Possible alternatives will be briefly considered: (i) Protonation of photoexcited diazo compounds might give diazonium ions and hence carbocations. As a consequence of this process, the quantum yields of photodecomposition in protic solvents should exceed those in aprotic solvents, which is not observed.[3] Our results with tetraphenyloxirane and 9-diazofluorene also argue against this mechanism. (ii) Photoexcitation of triplet carbenes might lead to excited triplet states which are known to behave very much like singlets.[21-24] The yield of carbocation was found to increase linearly with the intensity of the laser pulse. Thus one photon is sufficient to generate the carbocation precursor whereas two photons would be required to obtain the excited triplet state.

In summary, our data strongly support the protonation of singlet diarylcarbenes by ROH (eq 1, path a), a process that can compete efficiently with intersystem crossing to the triplet state.

(12) McClelland, R. A.; Banait, N.; Steenken, S. *J. Am. Chem. Soc.* **1989**, *111*, 2929.
(13) McClelland, R. A.; Kanagasabapathy, V. M.; Banait, N. S.; Steenken, S. *J. Am. Chem. Soc.* **1989**, *111*, 3966.
(14) Mecklenburg, S. L.; Hilinski, E. F. *J. Am. Chem. Soc.* **1989**, *111*, 5471.
(15) Johnston, L. J.; Lobaugh, J.; Wintgens, V. *J. Phys. Chem.* **1989**, *93*, 7370.
(16) Alonso, E. O.; Johnston, L. J.; Scaiano, J. C.; Toscano, V. G. *J. Am. Chem. Soc.* **1990**, *112*, 1270.
(17) Bartl, J.; Steenken, S.; Mayr, H.; McClelland, R. A. *J. Am. Chem. Soc.* **1990**, *112*.
(18) Trozzolo, A. M.; Yager, W. A.; Griffin, G. W.; Kristinsson, H.; Sarkar, I. *J. Am. Chem. Soc.* **1967**, *89*, 3357. Becker, R. S.; Kolc, J.; Bost, R. O.; Dietrich, H.; Petrellis, P.; Griffin, G. W. *Ibid.* **1968**, *90*, 3292. Becker, R. S.; Bost, R. O.; Kolc, J.; Bertoniere, N. R.; Smith, R. L.; Griffin, G. W. *Ibid.* **1970**, *92*, 1302.
(19) McClelland, R. A.; Mathivanan, N.; Steenken, S. *J. Am. Chem. Soc.* **1990**, *112*, 4857.
(20) Closs, G. L.; Rabinow, B. E. *J. Am. Chem. Soc.* **1976**, *98*, 8190.
(21) Sitzmann, E. V.; Wang, Y.; Eisenthal, K. B. *J. Phys. Chem.* **1983**, *87*, 2283.
(22) Johnston, L. J.; Scaiano, J. C. *Chem. Phys. Lett.* **1985**, *116*, 109.
(23) Horn, K. A.; Allison, B. D. *Chem. Phys. Lett.* **1985**, *116*, 114.
(24) Leyva, E.; Barcus, R. L.; Platz, M. S. *J. Am. Chem. Soc.* **1986**, *108*, 7786.

Easy, Reversible Addition of Mercury to Triplatinum Clusters: A Model for the First Step in Amalgamation of Platinum

Guy Schoettel, Jagadese J. Vittal, and Richard J. Puddephatt*

Department of Chemistry, University of Western Ontario London, Ontario, Canada N6A 5B7

Received May 2, 1990

The interaction of mercury atoms with metal surfaces is important, but it is difficult to study with most metals, including Pt, because of the ease of amalgamation.[1] Since there is a remarkable resemblance between the ways in which small molecules bind to the coordinatively unsaturated cluster complex $[Pt_3(\mu_3\text{-}CO)(\mu\text{-}dppm)_3]^{2+}$ (**1**), dppm = $Ph_2PCH_2PPh_2$, and a Pt(111) surface,[2] a study of mercury coordination to **1** should be a useful model for chemisorption of mercury atoms on a platinum surface which leads to PtHg amalgam. There has been theoretical work on $(Pt_3(CO)_6Hg)_\infty$ polymers,[3] which are predicted to have interesting physical properties, and of several known compounds with PtHg bonds,[4] the complexes $[\{Pt_3(\mu\text{-}L)_3L_3\}_2Hg]$, L = 2,6-

(1) Jones, R. G.; Tong, A. W. L. *Surf. Sci.* **1987**, *188*, 87.
(2) (a) Ferguson, G.; Lloyd, B. R.; Puddephatt, R. J. *Organometallics* **1986**, *5*, 344. (b) Douglas, G.; Jennings, M. C.; Manojlović-Muir, L.; Muir, K. W.; Puddephatt, R. J. *J. Chem. Soc., Chem. Commun.* **1989**, 159. (c) Ramachandran, R.; Payne, N. C.; Puddephatt, R. J. *J. Chem. Soc., Chem. Commun.* **1989**, 128. (d) Jennings, M. C.; Payne, N. C.; Puddephatt, R. J. *Inorg. Chem.* **1987**, *26*, 3776. (e) Lloyd, B. R.; Bradford, A.; Puddephatt, R. J. *Organometallics* **1987**, *6*, 424.
(3) Underwood, D. J.; Hoffmann, R.; Tatsumi, T.; Nakamura, A.; Yamamoto, Y. *J. Am. Chem. Soc.* **1985**, *107*, 5968.
(4) (a) Sharp, P. R. *Inorg. Chem.* **1986**, *25*, 4185. (b) Braunstein, P.; Rossell, O.; Seco, M.; Torra, I.; Solans, X.; Miravitlles, C. *Organometallics* **1986**, *5*, 113. (c) Ghilardi, C. A.; Midollini, S.; Moneti, S.; Orlandini, A.; Scapacci, G.; Dakternieks, D. *J. Chem. Soc., Chem. Commun.* **1989**, 1686.

0002-7863/90/1512-6400$02.50/0

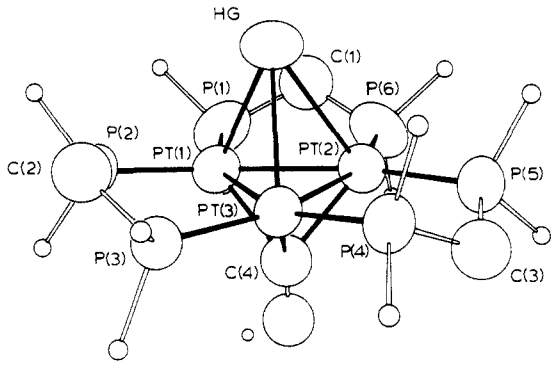

Figure 1. A view of the structure of the $[Pt_3(\mu_3\text{-Hg})(\mu_3\text{-CO})(\mu\text{-dppm})_3]^{2+}$ cation. Selected dimensions are Pt–Hg = 2.860 (1)–2.974 (1) Å, Pt–Pt = 2.626 (1)–2.645 (1) Å, Pt–C = 2.11 (2)–2.12 (2) Å, Pt–Hg–Pt = 52.79 (3)–54.31 (3)°. The mean Pt–Pt distances in **1**[2a] and **2** are 2.634 (2) and 2.639 (2) Å.

Scheme I

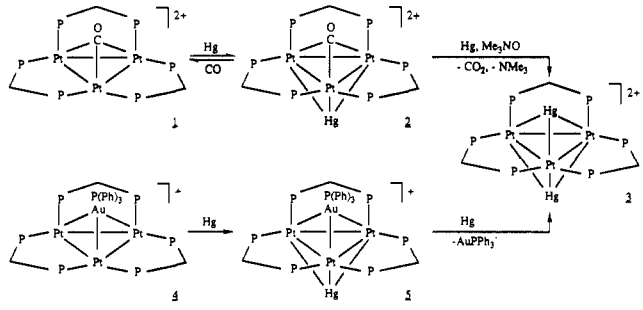

$Me_2C_6H_3NC$, which contains a mercury atom bridging two Pt_3 units,[5a] $[\{Pt_3(\mu\text{-CO})_3L_3Hg\}_2]$, L = PPh-*i*-$Pr_2$, which contains an Hg_2 unit bridging between two Pt_3 units,[5b,c] and $[Pt(AuPPh_3)_8Hg_2]^{4+}$, which contains two bare mercury atoms bound to a $PtAu_8$ cluster,[5d] are particularly relevant to the present work.

The new chemistry is shown in Scheme I, in which PP = dppm. Complex **1**, as the hexafluorophosphate salt, reacted easily with mercury at room temperature to give **2** in essentially quantitative yield, as monitored by UV–visible spectrophotometry or by ^1H and ^{31}P NMR spectroscopy.[6] Complex **2** is thermally stable, but it reacts with mercury in the presence of Me_3NO to give the bis(mercury) capped cluster **3**.[7] Complex **3** was also prepared by reaction of the $Pt_3(\mu_3\text{-AuPPh}_3)$ cluster **4** with excess mercury.[8] This reaction proceeds by way of the Pt_3AuHg cluster **5**, which was characterized by NMR spectroscopy but which could not be isolated in analytically pure form.[8] The $Pt_3(\mu_3\text{-Hg})$ linkages in **2** or **3** are labile and the mercury is easily displaced; for example, **2** or **3** reacts with excess CO to regenerate **1** (probably by way of the labile $[Pt_3(CO)_2(\mu\text{-dppm})_3]^{2+}$)[2e] and Hg, while **2** reacts with H_2S to give $[Pt_3H(\mu_3\text{-S})(\mu\text{-dppm})_3]^+$, CO, and Hg.[2d]

The structure of **2** was determined crystallographically and is shown in Figure 1.[9] It confirms the presence of a slightly distorted $Pt_3(\mu_3\text{-Hg})$ linkage, with d(Pt–Hg) = 2.859 (2) –2.970 (2) Å.

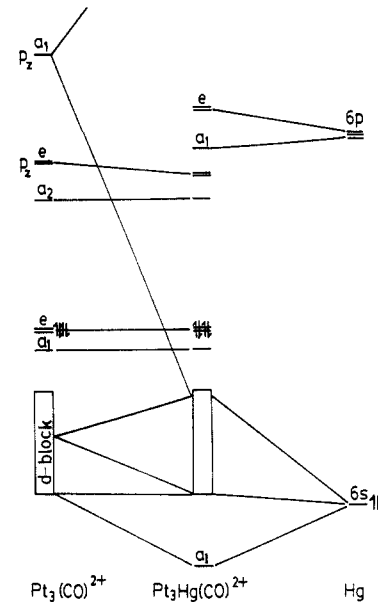

Figure 2. An interaction diagram for $[Pt_3(\mu_3\text{-CO})(\mu\text{-}H_2PCH_2PH_2)_3]^{2+}$ with Hg.

A molecular orbital analysis of the binding of mercury to the model complex $[Pt_3(\mu_3\text{-CO})(\mu\text{-}H_2PCH_2PH_2)_3]^{2+}$ has been made, and an interaction diagram is shown as Figure 2. The strongest interactions are calculated to be unfavorable ones between doubly occupied orbitals on both Hg (6s orbital) and Pt (filled d orbitals), but there is also a weak interaction of the Hg 6s orbital with the vacant a_1 (mostly $6p_z$) orbital on Pt which gives some stabilization. That this is a weak interaction is indicated by the very low calculated stabilization energy of –0.4 eV and small increase in platinum p_z occupation from 0.06e to 0.10e on addition of the Hg atom.[10] There is also calculated to be weak back-bonding from filled d orbitals on Pt to the empty $6p_\pi$ (e) orbitals of mercury, with the result that the mercury is calculated to be almost neutral (charge –0.06e). The frontier in-plane cluster orbitals [a_1 and e occupied; a_2 vacant on $Pt_3(CO)^{2+}$] are scarcely affected by the mercury binding. These results are fully consistent with the experimental observations, including the presence of long and presumably weak Pt–Hg bonds in **2**, the ease of displacement of Hg from **2**, and the modest change in the UV–visible spectrum and slight increase in the ν(CO) stretching frequency[6] on addition of Hg to **1**. Similar $Pt_3(\mu_3\text{-Hg})$ linkages may well be formed as the first step of adsorption of mercury on a platinum(111) surface leading to Pt–Hg amalgam.

Acknowledgment. We thank NSERC (Canada) for financial support, the University of Western Ontario for support of the X-ray facility, Dr. N. C. Payne for providing X-ray diffraction and computer facilities and computer programs, and Dr. D. S. Yang for assistance with the EHMO calculations.

Supplementary Material Available: Summary of X-ray structure determination and tables of atomic positional and thermal pa-

(5) (a) Albinati, A.; Moor, A.; Pregosin, P. S.; Venanzi, L. M. *J. Am. Chem. Soc.* **1982**, *104*, 1612. (b) Yamamoto, Y.; Yamazaki, H.; Sakurai, T. *J. Am. Chem. Soc.* **1982**, *104*, 2329. (c) Yamamoto, Y.; Yamazaki, H. *J. Chem. Soc., Dalton Trans.* **1989**, 2161. (d) Kanters, R. P. F.; Bour, J. J.; Schlebos, P. P. J.; Steggerda, J. J. *J. Chem. Soc., Chem. Commun.* **1988**, 1634.

(6) UV–visible spectra in MeOH: isosbestic points at 280 and 315 nm. NMR data for **2**: $\delta(^1H$, acetone-$d_6)$ = 5.65 and 6.20 [$^2J(H^aH^b)$ = 13, $CH^aH^bP_2$]; $\delta(^{13}C)$ = 196 [m, ^1J(PtC) = 854, ^2J(HgC) = 351, *C*O], obtained from a ^{13}C-enriched sample; $\delta(^{31}P)$ = –8.54 [m, ^1J(PtP) = 3763, ^2J(HgP) = 142, Pt*P*]; $\delta(^{195}Pt$, ref $K_2PtCl_4)$ = –2520 [^1J(PtP) = 3760]. IR data: ν(CO) = 1792 cm^{-1} [cf. ν(CO) = 1765 cm^{-1}, ^1J(PtC) = 777 Hz for **1**]. The synthesis of **2** was carried out in acetone solution.

(7) In the absence of Hg, the reaction of **2** with Me_3NO occurs with cluster fragmentation. For example, a reaction in CH_2Cl_2 solvent gave $[Pt_2Cl_2(\mu\text{-dppm})_2]$. NMR data for **3**: $\delta(^1H)$ = 5.48 [t, 6 H, ^2J(PH) = 25, CH_2]; $\delta(^{31}P)$ = 12.4 [s, ^1J(PtP) = 3384, ^2J(HgP) = 320, ^2J(PtP) = 17, ^3J(PP) = 119].

(8) NMR data for **5**: $\delta(^1H)$ = 5.26 and 5.67 [m, $^2J(H^aH^b)$ = 14, $CH^aH^bP_2$]; $\delta(^{31}P)$ = 16.3 [6 P, ^1J(PtP) = 2921, dppm]; 57.5 [1 P, ^2J(PtP) = 1022, ^3J(HgP) = 1404, Au*P*]. For comparison, **4** has $\delta(^{31}P)$ = 46.3 [^2J(PtP) = 892, Au*P*].

(9) Red crystals of $2\cdot(PF_6)_2\cdot C_7H_8\cdot 1.5CH_2Cl_2$ were grown from a mixture of toluene and dichloromethane. Crystal data for $C_{76}H_{66}OF_{12}HgP_8Pt_3\cdot C_7H_8\cdot 1.5CH_2Cl_2$: $P\bar{1}$, a = 16.159 (2) Å, b = 19.185 (2) Å, c = 15.955 (2) Å, α = 104.11 (1)°, β = 97.15 (1)°, γ = 100.58 (1)°, V = 4640 (2) Å^3, Z = 2, μ = 65.0 cm^{-1}, D_{calcd} = 1.78 (5) g cm^3; crystal dimensions 0.25 × 0.25 × 0.35 mm^3. Data were collected by using an Enraf-Nonius CAD4F diffractometer, with the crystal inside a capillary, using Mo Kα radiation; 12648 data were collected in the range 0° < 2θ < 45°; Gaussian absorption correction applied; in all, 12119 independent data. The structure was solved by MULTAN and subsequent diffractometer Fourier techniques. For 6503 observations ($I > 2.5\sigma$) and 343 variables, refinement converged at R_1 = 0.0534 and R_2 = 0.0563.

(10) Extended Hückel calculations using the averaged molecular dimensions for **2**. Parameters are as in ref 3. Much larger stabilization energies are calculated for $Pt_3(\mu\text{-CO})_3(CO)_3Hg$ and related compounds due to the presence of the equatorial π-acceptor CO ligands.[3]

rameters, anisotropic thermal parameters, hydrogen atom parameters, bond distances and angles, root-mean-square amplitudes of vibrations, and weighted least-squares planes and interplanar angles for $2\cdot(PF_6)_2\cdot C_7H_8\cdot 1.5CH_2Cl_2$ (14 pages); listing of observed and calculated structure amplitudes for $2\cdot(PF_6)_2\cdot C_7H_8\cdot 1.5CH_2Cl_2$ (39 pages). Ordering information is given on any current masthead page.

Synthetic Model for Dioxygen Binding Sites of Non-Heme Iron Proteins. X-ray Structure of Fe(OBz)(MeCN)(HB(3,5-iPr$_2$pz)$_3$) and Resonance Raman Evidence for Reversible Formation of a Peroxo Adduct

Nobumasa Kitajima,* Hideno Fukui, and Yoshihiko Moro-oka*

Research Laboratory of Resources Utilization
Tokyo Institute of Technology
4259 Nagatsuta, Midori-ku, Yokohama 227, Japan

Yasuhisa Mizutani and Teizo Kitagawa*

Institute of Molecular Science
Okazaki National Research Institutes
Department of Functional Molecular Science
The Graduate University for Advanced Studies
Myodaiji, Okazaki 444, Japan

Received January 16, 1990

The chemistry of dioxygen/porphyrin iron and related complexes continues to attract the attention of many chemists because of its relevance to biological systems.[1] On the contrary, little work has been done on the synthesis of dioxygen/non-porphyrin iron complexes,[2] although a family of non-heme iron containing oxygen carriers and oxygenases are now known. Among the proteins, the best characterized is hemerythrin, an oxygen carrier for some marine worms.[3] Although it contains a binuclear site, dioxygen binds only to one iron(II) center which is five-coordinate. The other non-heme proteins in this family, except methane monooxygenase, are known to contain a mononuclear iron site, and the coordination of multiple histidyl nitrogen atoms to iron has been suggested by analogy with hemerythrin. Our strategy for the development of a functional model for these non-heme iron proteins, therefore, lies in the synthesis of a mononuclear five-coordinate iron(II) complex by use of a hindered tris(pyrazolyl)borate ligand[4] which could allow us to see the binding of dioxygen at the open coordination site of the complex.[5] In this communication, we report the first success of such efforts.

The reaction of a tetrahedral iron(II) complex Fe(Cl)(HB(3,5-iPr$_2$pz)$_3$)[6] with an equimolar amount of NaOBz in toluene under argon gives a mononuclear complex, Fe(OBz)(HB(3,5-iPr$_2$pz)$_3$) (**1**).[7] Complex **1** is coordinatively unsaturated and accordingly reacts readily with MeCN or pyridine to yield the six-coordinate adduct. The crystal structure of Fe(OBz)(MeCN)(HB(3,5-iPr$_2$pz)$_3$) (**2**) was determined[8] and is shown in Figure 1. The benzoate group coordinates to the iron in a bidentate fashion, forming an octahedral coordination geometry.[9] The Fe–N bond lengths from the tris(pyrazolyl)borate ligand are similar to each other, with an average value of 2.14 Å, but significantly shorter than that of the MeCN ligand (2.28 Å). The

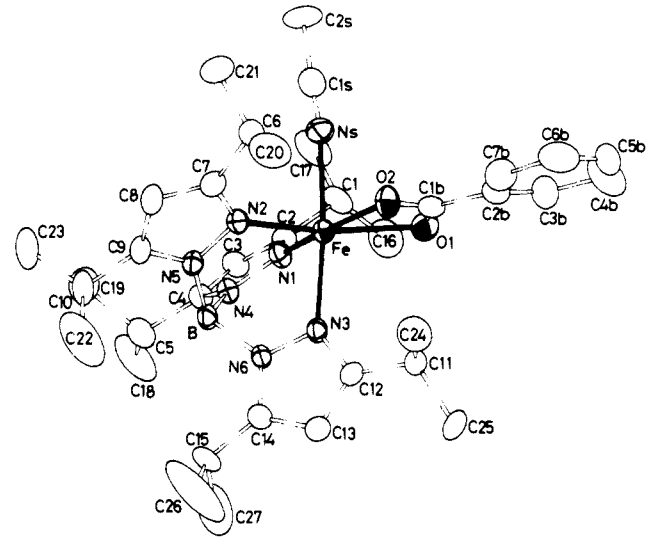

Figure 1. ORTEP view of **2**. Selected bond distances (Å) and angles (deg): Fe–O1, 2.252 (8); Fe–O2, 2.135 (8); Fe–Ns, 2.276 (9); Fe–N1, 2.116 (7); Fe–N2, 2.118 (7); Fe–N3, 2.196 (7); O1–C1b, 1.277 (16); O2–C1b, 1.215 (17); O1–Fe–O2, 59.2 (3); O1–C1b–O2, 121.0 (1.0); Ns–Fe–N1, 88.4 (3); Ns–Fe–N2, 90.2 (3); Ns–Fe–N3, 174.0 (3); Ns–Fe–O1, 86.1 (3); Ns–Fe–O2, 86.0 (3); Fe–Ns–C1s, 172.4 (9); N1–Fe–O1, 105.9 (3); N2–Fe–O2, 103.0 (3).

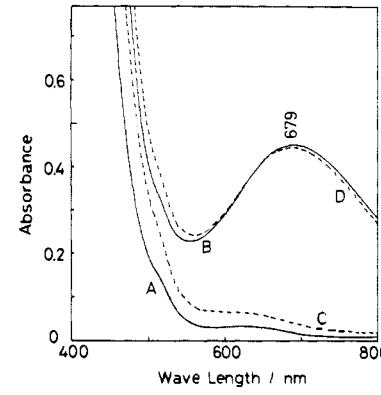

Figure 2. Electronic spectral changes of **1** in toluene under argon and dioxygen at −20 °C: (A) **1** in toluene under argon (concentration, 1.1 mM); (B) dioxygen is bubbled for 2 min in solution A; (C) argon is bubbled for 15 min in B; (D) dioxygen is bubbled for 2 min in C.

(1) Jones, R. D.; Summerville, D. A.; Basolo, F. *Chem. Rev.* **1979**, *79*, 139.
(2) (a) Baldwin, J. E.; Huff, J. *J. Am. Chem. Soc.* **1973**, *95*, 5757. (b) Marini, P. J.; Murray, K. S.; West, B. O. *J. Chem. Soc., Chem. Commun.* **1981**, 726. (c) Kimura, E.; Kodama, M.; Machida, R.; Ishizu, K. *Inorg. Chem.* **1982**, *21*, 595. (d) Herron, N.; Cameron, J. H.; Neer, G. L.; Busch, D. H. *J. Am. Chem. Soc.* **1983**, *105*, 298.
(3) (a) Wilkins, P. C.; Wilkins, R. G. *Coord. Chem. Rev.* **1987**, *79*, 195. (b) Lippard, S. J. *Angew. Chem., Int. Ed. Engl.* **1988**, *27*, 344.
(4) Kitajima, N.; Fujisawa, K.; Fujimoto, C.; Moro-oka, Y. *Chem. Lett.* **1989**, 421.
(5) As an accurate hemerythrin model, an asymmetric binuclear iron(II) complex which contains a five-coordinate iron was recently reported: Tolman, W. B.; Bino, A.; Lippard, S. J. *J. Am. Chem. Soc.* **1989**, *111*, 8522.
(6) Fe(Cl)(HB(3,5-iPr$_2$pz)$_3$) was synthesized by the reaction of $FeCl_2$ and KHB(3,5-iPr$_2$pz)$_3$ in CH_2Cl_2: Kitajima, N.; Fukui, H.; Moro-oka, Y. *Inorg. Chim. Acta*, submitted for publication.
(7) Abbreviations used: HB(3,5-iPr$_2$pz)$_3$, hydrotris(3,5-diisopropyl-1-pyrazolyl)borate; OBz, benzoate. Anal. Calcd for $C_{34}H_{51}N_6O_2BFe$: C, 63.56; H, 8.00; N, 13.08. Found for **1**: C, 62.83; H, 8.20; N, 12.84. IR (KBr, cm^{-1}): ν(HB), 2533; ν_a(COO), 1538; ν_s(COO), 1418.
(8) Recrystallization of **1** from MeCN at −20 °C yielded **2** as slightly yellow needles. Anal. Calcd for $C_{36}H_{54}N_7O_2BFe$: C, 63.26; H, 7.96; N, 14.34. Found for **3**: C, 63.18; H, 8.17; N, 14.75. IR (KBr, cm^{-1}): ν(BH), 2531; ν(CN), 2281; ν_a(COO), 1537; ν_s(COO), 1418. Magnetic susceptibility, solid state at 25 °C, 5.35 μ_B. **2** (FW, 683.53) crystallizes in the monoclinic space group $P2_1/n$ with a = 26.007 (10) Å, b = 15.320 (3) Å, c = 9.936 (3) Å, β = 93.93 (2)°, V = 3950 (2) Å^3, Z = 4. The structure was solved by direct methods and refined by full-matrix least squares with anisotropic thermal parameters for all non-hydrogen atoms. Hydrogen atoms except the ones on the methyl groups were calculated and fixed in the final refinements with d(C–H), 1.0 Å. The final R and R_w values are 8.97 and 9.15%, respectively, for 4075 independent reflections ($2° < 2\theta < 55°$, $F_o > 3\sigma(F_o)$).
(9) The structure is very similar to the active site of Fe-SOD: Ringe, D.; Petsko, G. A.; Yamakura, F.; Suzuki, K.; Ohmori, D. *Proc. Natl. Acad. Sci. U.S.A.* **1983**, *80*, 3879. Very recently, coordination of a carboxylato group to iron in a bidentate fashion was found in ribonucleotide reductase: Sahlin, M.; Nordlund, P.; Eklund, H.; Sjöberg, B.-M. *J. Inorg. Biochem.* **1989**, *36*, 228. Thus, complexes **1** and **2** are potentially good synthetic models for a wide variety of non-heme iron proteins (see other examples: Armstrong, W. H. *Metal Clusters in Proteins*; Que, L., Jr., Ed.; ACS Symposium Series 372; American Chemical Society: Washington, DC, 1988; Chapter 1.

0002-7863/90/1512-6402$02.50/0